BABAR-CONF-04/26
SLAC-PUB-10611
hep-ex/0408091
July 2004

A Search for $B^+ \to \tau^+\nu_\tau$ Recoiling Against $B^- \to D^{*0}\ell^-\overline{\nu}_\ell$

The *BABAR* Collaboration

August 18, 2004

Abstract

We present a search for the decay $B^+ \to \tau^+\nu_\tau$ in 124.1×10^6 $\Upsilon(4S)$ decays recorded with the *BABAR* detector at the SLAC PEP-II B-Factory. A sample of events with one reconstructed exclusive semi-leptonic B decay ($B^- \to D^{*0}\ell^-\overline{\nu}_\ell$) is selected, and in the recoil a search for $B^+ \to \tau^+\nu_\tau$ signal is performed. The τ is identified in the following channels: $\tau^+ \to e^+\nu_e\overline{\nu}_\tau$, $\tau^+ \to \mu^+\nu_\mu\overline{\nu}_\tau$, $\tau^+ \to \pi^+\overline{\nu}_\tau$, $\tau^+ \to \pi^+\pi^0\overline{\nu}_\tau$, $\tau^+ \to \pi^+\pi^-\pi^+\overline{\nu}_\tau$. We find no evidence of signal, and we set a preliminary upper limit on the branching fraction of $\mathcal{B}(B^+ \to \tau^+\nu_\tau) < 4.3 \times 10^{-4}$ at the 90% confidence level (CL). This result is then combined with a statistically independent *BABAR* search for $B^+ \to \tau^+\nu_\tau$ to give a combined preliminary limit of $\mathcal{B}(B^+ \to \tau^+\nu_\tau) < 3.3 \times 10^{-4}$ at 90% CL.

Submitted to the 32nd International Conference on High-Energy Physics, ICHEP 04,
16 August—22 August 2004, Beijing, China

Stanford Linear Accelerator Center, Stanford University, Stanford, CA 94309

Work supported in part by Department of Energy contract DE-AC03-76SF00515.

The *BABAR* Collaboration,

B. Aubert, R. Barate, D. Boutigny, F. Couderc, J.-M. Gaillard, A. Hicheur, Y. Karyotakis, J. P. Lees, V. Tisserand, A. Zghiche

Laboratoire de Physique des Particules, F-74941 Annecy-le-Vieux, France

A. Palano, A. Pompili

Università di Bari, Dipartimento di Fisica and INFN, I-70126 Bari, Italy

J. C. Chen, N. D. Qi, G. Rong, P. Wang, Y. S. Zhu

Institute of High Energy Physics, Beijing 100039, China

G. Eigen, I. Ofte, B. Stugu

University of Bergen, Inst. of Physics, N-5007 Bergen, Norway

G. S. Abrams, A. W. Borgland, A. B. Breon, D. N. Brown, J. Button-Shafer, R. N. Cahn, E. Charles, C. T. Day, M. S. Gill, A. V. Gritsan, Y. Groysman, R. G. Jacobsen, R. W. Kadel, J. Kadyk, L. T. Kerth, Yu. G. Kolomensky, G. Kukartsev, G. Lynch, L. M. Mir, P. J. Oddone, T. J. Orimoto, M. Pripstein, N. A. Roe, M. T. Ronan, V. G. Shelkov, W. A. Wenzel

Lawrence Berkeley National Laboratory and University of California, Berkeley, CA 94720, USA

M. Barrett, K. E. Ford, T. J. Harrison, A. J. Hart, C. M. Hawkes, S. E. Morgan, A. T. Watson

University of Birmingham, Birmingham, B15 2TT, United Kingdom

M. Fritsch, K. Goetzen, T. Held, H. Koch, B. Lewandowski, M. Pelizaeus, M. Steinke

Ruhr Universität Bochum, Institut für Experimentalphysik 1, D-44780 Bochum, Germany

J. T. Boyd, N. Chevalier, W. N. Cottingham, M. P. Kelly, T. E. Latham, F. F. Wilson

University of Bristol, Bristol BS8 1TL, United Kingdom

T. Cuhadar-Donszelmann, C. Hearty, N. S. Knecht, T. S. Mattison, J. A. McKenna, D. Thiessen

University of British Columbia, Vancouver, BC, Canada V6T 1Z1

A. Khan, P. Kyberd, L. Teodorescu

Brunel University, Uxbridge, Middlesex UB8 3PH, United Kingdom

A. E. Blinov, V. E. Blinov, V. P. Druzhinin, V. B. Golubev, V. N. Ivanchenko, E. A. Kravchenko, A. P. Onuchin, S. I. Serednyakov, Yu. I. Skovpen, E. P. Solodov, A. N. Yushkov

Budker Institute of Nuclear Physics, Novosibirsk 630090, Russia

D. Best, M. Bruinsma, M. Chao, I. Eschrich, D. Kirkby, A. J. Lankford, M. Mandelkern, R. K. Mommsen, W. Roethel, D. P. Stoker

University of California at Irvine, Irvine, CA 92697, USA

C. Buchanan, B. L. Hartfiel

University of California at Los Angeles, Los Angeles, CA 90024, USA

S. D. Foulkes, J. W. Gary, B. C. Shen, K. Wang

University of California at Riverside, Riverside, CA 92521, USA

D. del Re, H. K. Hadavand, E. J. Hill, D. B. MacFarlane, H. P. Paar, Sh. Rahatlou, V. Sharma

University of California at San Diego, La Jolla, CA 92093, USA

J. W. Berryhill, C. Campagnari, B. Dahmes, O. Long, A. Lu, M. A. Mazur, J. D. Richman, W. Verkerke

University of California at Santa Barbara, Santa Barbara, CA 93106, USA

T. W. Beck, A. M. Eisner, C. A. Heusch, J. Kroseberg, W. S. Lockman, G. Nesom, T. Schalk, B. A. Schumm, A. Seiden, P. Spradlin, D. C. Williams, M. G. Wilson

University of California at Santa Cruz, Institute for Particle Physics, Santa Cruz, CA 95064, USA

J. Albert, E. Chen, G. P. Dubois-Felsmann, A. Dvoretskii, D. G. Hitlin, I. Narsky, T. Piatenko, F. C. Porter, A. Ryd, A. Samuel, S. Yang

California Institute of Technology, Pasadena, CA 91125, USA

S. Jayatilleke, G. Mancinelli, B. T. Meadows, M. D. Sokoloff

University of Cincinnati, Cincinnati, OH 45221, USA

T. Abe, F. Blanc, P. Bloom, S. Chen, W. T. Ford, U. Nauenberg, A. Olivas, P. Rankin, J. G. Smith, J. Zhang, L. Zhang

University of Colorado, Boulder, CO 80309, USA

A. Chen, J. L. Harton, A. Soffer, W. H. Toki, R. J. Wilson, Q. Zeng

Colorado State University, Fort Collins, CO 80523, USA

D. Altenburg, T. Brandt, J. Brose, M. Dickopp, E. Feltresi, A. Hauke, H. M. Lacker, R. Müller-Pfefferkorn, R. Nogowski, S. Otto, A. Petzold, J. Schubert, K. R. Schubert, R. Schwierz, B. Spaan, J. E. Sundermann

Technische Universität Dresden, Institut für Kern- und Teilchenphysik, D-01062 Dresden, Germany

D. Bernard, G. R. Bonneaud, F. Brochard, P. Grenier, S. Schrenk, Ch. Thiebaux, G. Vasileiadis, M. Verderi

Ecole Polytechnique, LLR, F-91128 Palaiseau, France

D. J. Bard, P. J. Clark, D. Lavin, F. Muheim, S. Playfer, Y. Xie

University of Edinburgh, Edinburgh EH9 3JZ, United Kingdom

M. Andreotti, V. Azzolini, D. Bettoni, C. Bozzi, R. Calabrese, G. Cibinetto, E. Luppi, M. Negrini, L. Piemontese, A. Sarti

Università di Ferrara, Dipartimento di Fisica and INFN, I-44100 Ferrara, Italy

E. Treadwell

Florida A&M University, Tallahassee, FL 32307, USA

F. Anulli, R. Baldini-Ferroli, A. Calcaterra, R. de Sangro, G. Finocchiaro, P. Patteri, I. M. Peruzzi, M. Piccolo, A. Zallo

Laboratori Nazionali di Frascati dell'INFN, I-00044 Frascati, Italy

A. Buzzo, R. Capra, R. Contri, G. Crosetti, M. Lo Vetere, M. Macri, M. R. Monge, S. Passaggio, C. Patrignani, E. Robutti, A. Santroni, S. Tosi

Università di Genova, Dipartimento di Fisica and INFN, I-16146 Genova, Italy

S. Bailey, G. Brandenburg, K. S. Chaisanguanthum, M. Morii, E. Won

Harvard University, Cambridge, MA 02138, USA

R. S. Dubitzky, U. Langenegger

Universität Heidelberg, Physikalisches Institut, Philosophenweg 12, D-69120 Heidelberg, Germany

W. Bhimji, D. A. Bowerman, P. D. Dauncey, U. Egede, J. R. Gaillard, G. W. Morton, J. A. Nash, M. B. Nikolich, G. P. Taylor

Imperial College London, London, SW7 2AZ, United Kingdom

M. J. Charles, G. J. Grenier, U. Mallik

University of Iowa, Iowa City, IA 52242, USA

J. Cochran, H. B. Crawley, J. Lamsa, W. T. Meyer, S. Prell, E. I. Rosenberg, A. E. Rubin, J. Yi

Iowa State University, Ames, IA 50011-3160, USA

M. Biasini, R. Covarelli, M. Pioppi

Università di Perugia, Dipartimento di Fisica and INFN, I-06100 Perugia, Italy

M. Davier, X. Giroux, G. Grosdidier, A. Höcker, S. Laplace, F. Le Diberder, V. Lepeltier, A. M. Lutz, T. C. Petersen, S. Plaszczynski, M. H. Schune, L. Tantot, G. Wormser

Laboratoire de l'Accélérateur Linéaire, F-91898 Orsay, France

C. H. Cheng, D. J. Lange, M. C. Simani, D. M. Wright

Lawrence Livermore National Laboratory, Livermore, CA 94550, USA

A. J. Bevan, C. A. Chavez, J. P. Coleman, I. J. Forster, J. R. Fry, E. Gabathuler, R. Gamet, D. E. Hutchcroft, R. J. Parry, D. J. Payne, R. J. Sloane, C. Touramanis

University of Liverpool, Liverpool L69 72E, United Kingdom

J. J. Back,[1] C. M. Cormack, P. F. Harrison,[1] F. Di Lodovico, G. B. Mohanty[1]

Queen Mary, University of London, E1 4NS, United Kingdom

C. L. Brown, G. Cowan, R. L. Flack, H. U. Flaecher, M. G. Green, P. S. Jackson, T. R. McMahon, S. Ricciardi, F. Salvatore, M. A. Winter

University of London, Royal Holloway and Bedford New College, Egham, Surrey TW20 0EX, United Kingdom

D. Brown, C. L. Davis

University of Louisville, Louisville, KY 40292, USA

J. Allison, N. R. Barlow, R. J. Barlow, P. A. Hart, M. C. Hodgkinson, G. D. Lafferty, A. J. Lyon, J. C. Williams

University of Manchester, Manchester M13 9PL, United Kingdom

A. Farbin, W. D. Hulsbergen, A. Jawahery, D. Kovalskyi, C. K. Lae, V. Lillard, D. A. Roberts

University of Maryland, College Park, MD 20742, USA

G. Blaylock, C. Dallapiccola, K. T. Flood, S. S. Hertzbach, R. Kofler, V. B. Koptchev, T. B. Moore, S. Saremi, H. Staengle, S. Willocq

University of Massachusetts, Amherst, MA 01003, USA

[1]Now at Department of Physics, University of Warwick, Coventry, United Kingdom

R. Cowan, G. Sciolla, S. J. Sekula, F. Taylor, R. K. Yamamoto

Massachusetts Institute of Technology, Laboratory for Nuclear Science, Cambridge, MA 02139, USA

D. J. J. Mangeol, P. M. Patel, S. H. Robertson

McGill University, Montréal, QC, Canada H3A 2T8

A. Lazzaro, V. Lombardo, F. Palombo

Università di Milano, Dipartimento di Fisica and INFN, I-20133 Milano, Italy

J. M. Bauer, L. Cremaldi, V. Eschenburg, R. Godang, R. Kroeger, J. Reidy, D. A. Sanders, D. J. Summers, H. W. Zhao

University of Mississippi, University, MS 38677, USA

S. Brunet, D. Côté, P. Taras

Université de Montréal, Laboratoire René J. A. Lévesque, Montréal, QC, Canada H3C 3J7

H. Nicholson

Mount Holyoke College, South Hadley, MA 01075, USA

N. Cavallo,[2] F. Fabozzi,[2] C. Gatto, L. Lista, D. Monorchio, P. Paolucci, D. Piccolo, C. Sciacca

Università di Napoli Federico II, Dipartimento di Scienze Fisiche and INFN, I-80126, Napoli, Italy

M. Baak, H. Bulten, G. Raven, H. L. Snoek, L. Wilden

NIKHEF, National Institute for Nuclear Physics and High Energy Physics, NL-1009 DB Amsterdam, The Netherlands

C. P. Jessop, J. M. LoSecco

University of Notre Dame, Notre Dame, IN 46556, USA

T. Allmendinger, K. K. Gan, K. Honscheid, D. Hufnagel, H. Kagan, R. Kass, T. Pulliam, A. M. Rahimi, R. Ter-Antonyan, Q. K. Wong

Ohio State University, Columbus, OH 43210, USA

J. Brau, R. Frey, O. Igonkina, C. T. Potter, N. B. Sinev, D. Strom, E. Torrence

University of Oregon, Eugene, OR 97403, USA

F. Colecchia, A. Dorigo, F. Galeazzi, M. Margoni, M. Morandin, M. Posocco, M. Rotondo, F. Simonetto, R. Stroili, G. Tiozzo, C. Voci

Università di Padova, Dipartimento di Fisica and INFN, I-35131 Padova, Italy

M. Benayoun, H. Briand, J. Chauveau, P. David, Ch. de la Vaissière, L. Del Buono, O. Hamon, M. J. J. John, Ph. Leruste, J. Malcles, J. Ocariz, M. Pivk, L. Roos, S. T'Jampens, G. Therin

Universités Paris VI et VII, Laboratoire de Physique Nucléaire et de Hautes Energies, F-75252 Paris, France

P. F. Manfredi, V. Re

Università di Pavia, Dipartimento di Elettronica and INFN, I-27100 Pavia, Italy

[2]Also with Università della Basilicata, Potenza, Italy

P. K. Behera, L. Gladney, Q. H. Guo, J. Panetta

University of Pennsylvania, Philadelphia, PA 19104, USA

C. Angelini, G. Batignani, S. Bettarini, M. Bondioli, F. Bucci, G. Calderini, M. Carpinelli, F. Forti, M. A. Giorgi, A. Lusiani, G. Marchiori, F. Martinez-Vidal,[3] M. Morganti, N. Neri, E. Paoloni, M. Rama, G. Rizzo, F. Sandrelli, J. Walsh

Università di Pisa, Dipartimento di Fisica, Scuola Normale Superiore and INFN, I-56127 Pisa, Italy

M. Haire, D. Judd, K. Paick, D. E. Wagoner

Prairie View A&M University, Prairie View, TX 77446, USA

N. Danielson, P. Elmer, Y. P. Lau, C. Lu, V. Miftakov, J. Olsen, A. J. S. Smith, A. V. Telnov

Princeton University, Princeton, NJ 08544, USA

F. Bellini, G. Cavoto,[4] R. Faccini, F. Ferrarotto, F. Ferroni, M. Gaspero, L. Li Gioi, M. A. Mazzoni, S. Morganti, M. Pierini, G. Piredda, F. Safai Tehrani, C. Voena

Università di Roma La Sapienza, Dipartimento di Fisica and INFN, I-00185 Roma, Italy

S. Christ, G. Wagner, R. Waldi

Universität Rostock, D-18051 Rostock, Germany

T. Adye, N. De Groot, B. Franek, N. I. Geddes, G. P. Gopal, E. O. Olaiya

Rutherford Appleton Laboratory, Chilton, Didcot, Oxon, OX11 0QX, United Kingdom

R. Aleksan, S. Emery, A. Gaidot, S. F. Ganzhur, P.-F. Giraud, G. Hamel de Monchenault, W. Kozanecki, M. Legendre, G. W. London, B. Mayer, G. Schott, G. Vasseur, Ch. Yèche, M. Zito

DSM/Dapnia, CEA/Saclay, F-91191 Gif-sur-Yvette, France

M. V. Purohit, A. W. Weidemann, J. R. Wilson, F. X. Yumiceva

University of South Carolina, Columbia, SC 29208, USA

D. Aston, R. Bartoldus, N. Berger, A. M. Boyarski, O. L. Buchmueller, R. Claus, M. R. Convery, M. Cristinziani, G. De Nardo, D. Dong, J. Dorfan, D. Dujmic, W. Dunwoodie, E. E. Elsen, S. Fan, R. C. Field, T. Glanzman, S. J. Gowdy, T. Hadig, V. Halyo, C. Hast, T. Hryn'ova, W. R. Innes, M. H. Kelsey, P. Kim, M. L. Kocian, D. W. G. S. Leith, J. Libby, S. Luitz, V. Luth, H. L. Lynch, H. Marsiske, R. Messner, D. R. Muller, C. P. O'Grady, V. E. Ozcan, A. Perazzo, M. Perl, S. Petrak, B. N. Ratcliff, A. Roodman, A. A. Salnikov, R. H. Schindler, J. Schwiening, G. Simi, A. Snyder, A. Soha, J. Stelzer, D. Su, M. K. Sullivan, J. Va'vra, S. R. Wagner, M. Weaver, A. J. R. Weinstein, W. J. Wisniewski, M. Wittgen, D. H. Wright, A. K. Yarritu, C. C. Young

Stanford Linear Accelerator Center, Stanford, CA 94309, USA

P. R. Burchat, A. J. Edwards, T. I. Meyer, B. A. Petersen, C. Roat

Stanford University, Stanford, CA 94305-4060, USA

S. Ahmed, M. S. Alam, J. A. Ernst, M. A. Saeed, M. Saleem, F. R. Wappler

State University of New York, Albany, NY 12222, USA

[3]Also with IFIC, Instituto de Física Corpuscular, CSIC-Universidad de Valencia, Valencia, Spain
[4]Also with Princeton University, Princeton, USA

W. Bugg, M. Krishnamurthy, S. M. Spanier
University of Tennessee, Knoxville, TN 37996, USA

R. Eckmann, H. Kim, J. L. Ritchie, A. Satpathy, R. F. Schwitters
University of Texas at Austin, Austin, TX 78712, USA

J. M. Izen, I. Kitayama, X. C. Lou, S. Ye
University of Texas at Dallas, Richardson, TX 75083, USA

F. Bianchi, M. Bona, F. Gallo, D. Gamba
Università di Torino, Dipartimento di Fisica Sperimentale and INFN, I-10125 Torino, Italy

L. Bosisio, C. Cartaro, F. Cossutti, G. Della Ricca, S. Dittongo, S. Grancagnolo, L. Lanceri, P. Poropat,[5] L. Vitale, G. Vuagnin
Università di Trieste, Dipartimento di Fisica and INFN, I-34127 Trieste, Italy

R. S. Panvini
Vanderbilt University, Nashville, TN 37235, USA

Sw. Banerjee, C. M. Brown, D. Fortin, P. D. Jackson, R. Kowalewski, J. M. Roney, R. J. Sobie
University of Victoria, Victoria, BC, Canada V8W 3P6

H. R. Band, B. Cheng, S. Dasu, M. Datta, A. M. Eichenbaum, M. Graham, J. J. Hollar, J. R. Johnson, P. E. Kutter, H. Li, R. Liu, A. Mihalyi, A. K. Mohapatra, Y. Pan, R. Prepost, P. Tan, J. H. von Wimmersperg-Toeller, J. Wu, S. L. Wu, Z. Yu
University of Wisconsin, Madison, WI 53706, USA

M. G. Greene, H. Neal
Yale University, New Haven, CT 06511, USA

[5]Deceased

1 INTRODUCTION

In the Standard Model (SM), the purely leptonic decay $B^+ \to \tau^+\nu_\tau$ [6] proceeds via quark annihilation into a W^+ boson (Fig. 1). Its amplitude is thus proportional to the product of the B-decay constant f_B and the quark-mixing-matrix element V_{ub}. The branching fraction is given by:

$$\mathcal{B}(B^+ \to \tau^+\nu) = \frac{G_F^2 m_B m_\tau^2}{8\pi}\left[1 - \frac{m_\tau^2}{m_B^2}\right]^2 \tau_{B^+} f_B^2 \mid V_{ub} \mid^2, \tag{1}$$

where we have set $\hbar = c = 1$, G_F is the Fermi constant, V_{ub} is a quark mixing matrix element [1, 2], f_B is the B^+ meson decay constant which describes the overlap of the quark wave-functions inside the meson, τ_{B^+} is the B^+ lifetime, and m_B and m_τ are the B^+ meson and τ masses. This expression is entirely analogous to that for pion decay. Physics beyond the SM, such as supersymmetry or two-Higgs doublet models, could enhance $\mathcal{B}(B^+ \to \tau^+\nu_\tau)$ by up to a factor of five through the introduction of a charged Higgs boson [3].

Current theoretical values for f_B (obtained from lattice QCD calculations) [4] have large uncertainty, and purely leptonic decays of the B^+ meson may be the only clean experimental method of measuring f_B precisely. Given measurements of $|V_{ub}|$ from semi-leptonic processes such as $B \to \pi\ell\nu$, f_B could be extracted from the measurement of the $B^+ \to \tau^+\nu_\tau$ branching fraction. In addition, by combining the branching fraction measurement with results from B mixing, the ratio $|V_{ub}|/|V_{td}|$ can be extracted from $\mathcal{B}(B^+ \to \tau^+\nu_\tau)/\Delta m$, where Δm is the mass difference between the heavy and light neutral B meson states.

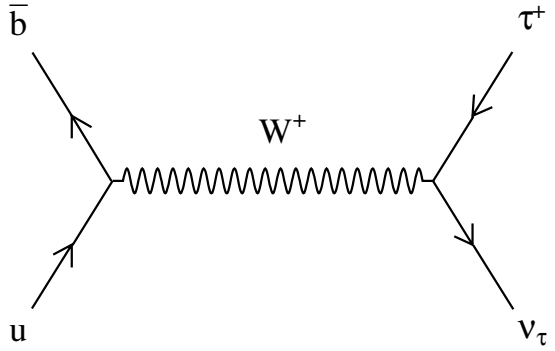

Figure 1: Purely leptonic B decay $B^+ \to \tau^+\nu_\tau$ proceeds via quark annihilation into a W^+ boson.

The decay amplitude is proportional to the lepton mass and decay to the lighter leptons is severely suppressed. This mode is therefore the most promising for discovery at existing experiments. However, challenges such as the large missing momentum from several neutrinos make the signature for $B^+ \to \tau^+\nu_\tau$ less distinctive than for other leptonic modes.

The SM estimate of this branching fraction is $(9.3\pm3.9)\times10^{-5}$, using $|V_{ub}| = (3.67\pm0.47)\times10^{-4}$ and $f_B = 0.196 \pm 0.032$ [4] in Eq. 1.

Purely leptonic B decays have not yet been observed. CLEO [5] and experiments at LEP [6, 7, 8] have searched for this process and set limits on the branching fraction at the 90% CL. The most

[6] Charge-conjugate modes are implied throughout this paper. The signal B will always be denoted as a B^+ decay while the semi-leptonic B will be denoted as a B^- to avoid confusion.

stringent limit on $\mathcal{B}(B^+ \to \tau^+\nu_\tau)$ comes from the L3 experiment [6]:

$$\mathcal{B}(B^+ \to \tau^+\nu_\tau) \quad < \quad 5.7 \times 10^{-4} \text{ at the 90\% CL.} \tag{2}$$

The *BABAR* collaboration has results on the search for $B^+ \to \tau^+\nu_\tau$ decays [9] using a sample of 88.9×10^6 $\Upsilon(4S)$ decays; the upper limit is:

$$\mathcal{B}(B^+ \to \tau^+\nu_\tau) \quad < \quad 4.2 \times 10^{-4} \text{ at the 90\% CL.} \tag{3}$$

In this paper we report on a preliminary result from a different analysis on a larger dataset.

2 THE *BABAR* DETECTOR AND DATASET

The data used in this analysis were collected with the *BABAR* detector at the PEP-II storage ring. The sample corresponds to an integrated luminosity of $112.5\,\text{fb}^{-1}$ at the $\Upsilon(4S)$ resonance (on-resonance) and $11.9\,\text{fb}^{-1}$ taken 40 MeV below the $\Upsilon(4S)$ resonance (off-resonance). The on-resonance sample consists of about $(124.1 \pm 1.4) \times 10^6$ $\Upsilon(4S)$ decays ($B\overline{B}$ pairs). The collider is operated with asymmetric beam energies, producing a boost of $\beta\gamma \approx 0.56$ of the $\Upsilon(4S)$ along the collision axis.

The *BABAR* detector is optimized for asymmetric energy collisions at a center-of-mass (CM) energy corresponding to the $\Upsilon(4S)$ resonance. The detector is described in detail in reference [10]. Charged particle tracking is provided by a five-layer double-sided silicon vertex tracker (SVT) and a 40-layer drift chamber (DCH) contained within the magnetic field of a 1.5 T superconducting solenoid. The tracking system provides momentum reconstruction of charged particles and measures energy loss (dE/dx) for particle identification. Additional charged K–π particle identification is provided by a ring-imaging Cherenkov detector (DIRC), which exploits the total internal reflection of Cherenkov photons within the purified quartz bars. The energies of neutral particles are measured by an electromagnetic calorimeter (EMC) composed of 6580 CsI(Tl) crystals, which provides an energy resolution $\sigma_E/E = (2.3/E^{1/4} \oplus 1.9)\%$, where E is in GeV. For 20 MeV and 1 GeV clusters the EMC energy resolutions are ∼6% and ∼3%, respectively. The magnetic flux return of the solenoid (IFR) is instrumented with resistive plate chambers in order to provide muon and neutral hadron identification.

A GEANT4-based [11] Monte Carlo (MC) simulation is used to model the signal efficiency and the physics backgrounds. Simulation samples equivalent to approximately three times the accumulated data were used to model $B\overline{B}$ events, and samples equivalent to approximately 1.5 times the accumulated data were used to model $e^+e^- \to u\overline{u}$, $d\overline{d}$, $s\overline{s}$, $c\overline{c}$, and $\tau^+\tau^-$ events. A large sample of signal events is simulated, where one of the B meson decays to $B^+ \to \tau^+\nu_\tau$. Beam related background and detector noise from data are overlaid on the simulated events.

3 ANALYSIS METHOD

Due to the presence of multiple neutrinos, the $B^+ \to \tau^+\nu_\tau$ decay mode lacks the kinematic constraints which are usually exploited in B decay searches in order to reject both continuum and $B\overline{B}$ backgrounds. The strategy adopted for this analysis is to reconstruct exclusively the decay of one of the B mesons in the event, referred to as "tag" B, and to compare the remaining particle(s) in the event, referred as the "signal side", with the signature expected for the decay $B^+ \to \tau^+\nu_\tau$. In

order to avoid experimenter bias, the signal region in data is not examined ("blinded") until the selection is optimized based on MC simulation.

The tag B is reconstructed in the set of decay modes $B^- \to D^{*0}\ell^-\overline{\nu}_\ell$, where ℓ is e or μ. The D^{*0} is reconstructed in $D^0\pi^0$ and $D^0\gamma$ modes. The D^0 is reconstructed in four decay modes: $K^-\pi^+$, $K^-\pi^+\pi^-\pi^+$, $K^-\pi^+\pi^0$, and $K^0_s\pi^+\pi^-$. The K^0_s is reconstructed only in the mode $K^0_s \to \pi^+\pi^-$. On the signal side the $B^+ \to \tau^+\nu_\tau$ signal is searched for in both leptonic and hadronic τ decay modes: $\tau^+ \to e^+\nu_e\overline{\nu}_\tau$, $\tau^+ \to \mu^+\nu_\mu\overline{\nu}_\tau$, $\tau^+ \to \pi^+\overline{\nu}_\tau$, $\tau^+ \to \pi^+\pi^0\overline{\nu}_\tau$, $\tau^+ \to \pi^+\pi^-\pi^+\overline{\nu}_\tau$. The branching fractions of the above τ decay modes are listed in Table 1. Most of the kinematic variables used for event selection and background rejection are measured in the CM frame.

Table 1: Branching fractions for the τ decay modes used in the $B^+ \to \tau^+\nu_\tau$ search [4].

Decay Mode	Branching Fraction (%)
$\tau^+ \to e^+\nu_e\overline{\nu}_\tau$	17.84 ± 0.06
$\tau^+ \to \mu^+\nu_\mu\overline{\nu}_\tau$	17.36 ± 0.06
$\tau^+ \to \pi^+\overline{\nu}_\tau$	11.06 ± 0.11
$\tau^+ \to \pi^+\pi^0\overline{\nu}_\tau$	25.42 ± 0.14
$\tau^+ \to \pi^+\pi^-\pi^+\overline{\nu}_\tau$	9.16 ± 0.10

3.1 TAG B RECONSTRUCTION

The tag B reconstruction proceeds as follows. First we reconstruct the D^0 candidates in the above four decay modes using tracks and/or a π^0. The tracks are required to meet particle identification criteria consistent with the particle hypothesis, and are required to converge at a common vertex. The π^0 candidate is required to have invariant mass between 0.115–0.150 GeV/c^2 and its daughter photon candidates must have a minimum energy of 30 MeV. The mass of the reconstructed D^0 candidates in $K^-\pi^+$, $K^-\pi^+\pi^-\pi^+$, and $K^0_s\pi^+\pi^-$ modes are required to be within 40 MeV of the nominal mass [4]. In the $K^-\pi^+\pi^0$ decay mode the mass is required to be within 70 MeV of the nominal mass [4].

The D^{*0} candidates are reconstructed by combining the D^0 candidates with a soft π^0 or γ, whose momentum in the CM frame is less than 0.45 GeV/c. The mass difference between D^{*0} and D^0 (ΔM) is restricted to be within 0.13–0.17 GeV/c^2 and 0.12–0.17 GeV/c^2 for $D^0\pi^0$ and $D^0\gamma$ modes, respectively. We further require that the photon used in $D^{*0} \to D^0\gamma$ reconstruction has a minimum energy of 100 MeV.

Finally $D^{*0}\ell$ candidates are reconstructed by combining D^{*0} with an identified electron or muon of a momentum above 1.0 GeV/c in the CM frame. The D^{*0} and ℓ candidates are required to meet at a common vertex. An additional kinematic constraint is imposed on the reconstructed $D^{*0}\ell$ candidates: Assuming that the massless neutrino is the only missing particle, we calculate the cosine of the angle between the $D^{*0}\ell$ candidate and the B meson,

$$\cos\theta_{B-D^{*0}\ell} = \frac{2E_B E_{D^{*0}\ell} - m_B^2 - m_{D^{*0}\ell}^2}{2|\vec{p}_B||\vec{p}_{D^{*0}\ell}|}. \quad (4)$$

Here ($E_{D^{*0}\ell}$, $\vec{p}_{D^{*0}\ell}$) and (E_B, $\vec{p}_B$) are the four-momenta in the CM frame, and $m_{D^{*0}\ell}$ and m_B are the masses of the $D^{*0}\ell$ candidate and B meson, respectively. E_B and the magnitude of $\vec{p}_B$ are

calculated from the beam energy: $E_B = E_{\rm beam} = E_{\rm CM}/2$ and $|\vec{p}_B| = \sqrt{E^2_{\rm beam} - m^2_B}$. Correctly reconstructed candidates populate the range [-1,1], whereas combinatorial backgrounds can take unphysical values outside this range. We retain events in the interval $-1.1 < \cos\theta_{B-D^{*0}\ell} < 1.1$, to take into account the detector energy and momentum resolution.

If more than one suitable $D^{*0}\ell$ candidate is reconstructed in an event, the best candidate is selected based on the D^0 mass and ΔM. A two dimensional likelihood function is formed by taking the product of the D^0 mass and ΔM distributions obtained from MC simulation. We select the candidate with the largest likelihood.

The following additional cuts are applied on the selected best candidate. The ΔM value for the best candidate is required to be between 0.135–0.150 GeV/c^2 and 0.130–0.155 GeV/c^2 for candidates reconstructed in $D^0\pi^0$ and $D^0\gamma$ modes, respectively. The angle between the D^0 and the soft π^0 or γ from D^{*0} decay in the CM frame is restricted to be less than 60° and 90° for D^{*0} reconstructed in $D^0\pi^0$ and $D^0\gamma$ modes, respectively. The sum of the charge of all the particles in the event (net charge) must be equal to zero for events with selected candidates.

At this stage of the selection, the observed yield in data and the predicted yield in the MC simulation agree to within approximately 6%. This discrepancy is corrected by scaling the yield and efficiency obtained from MC simulation. The scale factor of 0.937 is used to correct the tag B reconstruction efficiency in the signal MC simulation. The systematic error associated with this correction will be described in Sec. 5. The corrected tag reconstruction efficiency in the signal MC simulation is $(1.818 \pm 0.074)\times10^{-3}$. Figure 2 shows the ΔM distributions of the selected best $D^{*0}e\nu$ candidates.

3.2 SELECTION OF $B^+ \to \tau^+\nu_\tau$ DECAYS

After the tag B reconstruction, in the signal side the τ from the $B^+ \to \tau^+\nu_\tau$ decay is identified in one of the following modes: $\tau^+ \to e^+\nu_e\overline{\nu}_\tau$, $\tau^+ \to \mu^+\nu_\mu\overline{\nu}_\tau$, $\tau^+ \to \pi^+\overline{\nu}_\tau$, $\tau^+ \to \pi^+\pi^0\overline{\nu}_\tau$, or $\tau^+ \to \pi^+\pi^-\pi^+\overline{\nu}_\tau$. We select events with one or three signal-side track(s). The event is rejected if any of the signal-side tracks fail the following selection criteria: it must have at least 12 DCH hits, its momentum transverse to the beam axis, $p_{\rm T}$, is greater than 0.1 GeV/c, and its point of closest approach to the interaction point is less than 10.0 cm along the beam axis and less than 1.5 cm transverse to the beam axis. Figure 3(a) shows the distribution of the number of signal-side tracks before this cut. The invariant mass of a signal-side π^0 candidate must be between 0.10–0.16 GeV/c^2, the shower shape of the daughter photon candidates must be consistent with an electromagnetic shower shape and the photons must have a minimum energy of 50 MeV.

The most powerful variable for separating signal and background is the remaining neutral energy ($E_{\rm extra}$), calculated by adding the CM energy of the photons that are not associated with either the tag B or the π^0 candidate from $\tau^+ \to \pi^+\pi^0\overline{\nu}_\tau$ signal decay. The photon candidates contributing to the $E_{\rm extra}$ variable have minimum cluster energies of 20 MeV. For signal events the neutral clusters contributing to $E_{\rm extra}$ can only come from processes like beam-background, hadronic split-offs, and bremsstrahlung. Therefore the signal events peak at low $E_{\rm extra}$ values and the background events, which contain additional sources of neutral clusters, are distributed towards higher $E_{\rm extra}$ values (see fig. 3(b)). The $E_{\rm extra} < 0.3$ GeV region is defined as the signal region. This $E_{\rm extra} < 0.35$ GeV region, which is slightly larger than the signal region, is kept blinded in on-resonance data until the selection is optimized.

The different signal modes are distinguished by the following selection criteria. The $\tau^+ \to e^+\nu_e\overline{\nu}_\tau$, $\tau^+ \to \mu^+\nu_\mu\overline{\nu}_\tau$, $\tau^+ \to \pi^+\overline{\nu}_\tau$, and $\tau^+ \to \pi^+\pi^0\overline{\nu}_\tau$ signal modes, all of which contain one

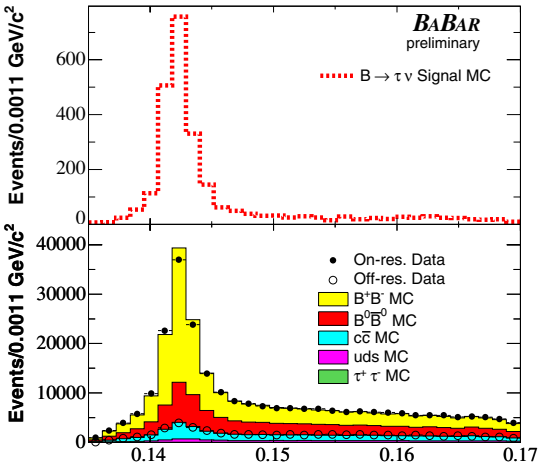

(a) The ΔM distribution of $D^{*0}(D^0\pi^0)e\nu$ candidate plotted for $B^+ \to \tau^+\nu_\tau$ signal simulation (top) and for data and background simulation (bottom).

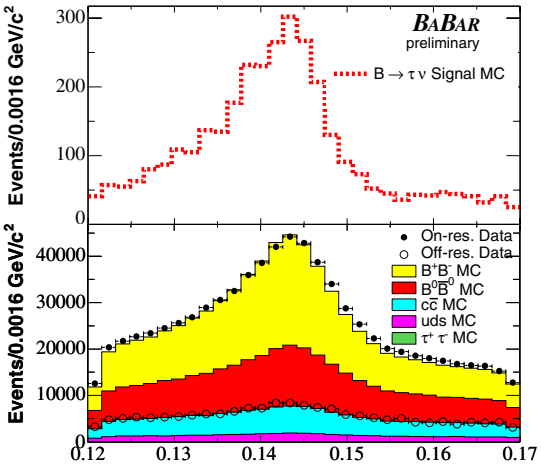

(b) The ΔM distribution of $D^{*0}(D^0\gamma)e\nu$ candidate plotted for $B^+ \to \tau^+\nu_\tau$ signal simulation (top) and for data and background simulation (bottom).

Figure 2: The ΔM distributions of $D^{*0}e\nu$ candidate with D^{*0} reconstructed in $D^0\pi^0$ (fig. 2(a)) and $D^0\gamma$ (fig. 2(b)) modes, plotted for $B^+ \to \tau^+\nu_\tau$ simulation, background simulation and data. The ΔM, and the angle between the D^0 and the soft π^0 or γ requirements are not applied on the $D^{*0}e\nu$ candidates plotted in these distributions. Here the simulated background events are scaled to match the data yield. The normalization of the signal MC events is arbitrary. These distributions are similar for the $D^{*0}\mu\nu$ candidates.

charged track, are separated by particle identification. Both the $\tau^+ \to \pi^+\overline{\nu}_\tau$ and the $\tau^+ \to \pi^+\pi^0\overline{\nu}_\tau$ modes contain a pion signal track and are characterized by the number of signal-side π^0 mesons. The $\tau^+ \to \pi^+\pi^-\pi^+\overline{\nu}_\tau$ mode contains three signal-side tracks. These signal selection requirements are as follows.

- Particle identification:
  - For the $\tau^+ \to e^+\nu_e\overline{\nu}_\tau$ selection the track must be identified as an electron and not identified as a muon or a kaon.
  - For the $\tau^+ \to \mu^+\nu_\mu\overline{\nu}_\tau$ selection the track must be identified as a muon and not identified as an electron or a kaon.
  - For the $\tau^+ \to \pi^+\overline{\nu}_\tau$ and $\tau^+ \to \pi^+\pi^0\overline{\nu}_\tau$ selection we require that the track is not identified as an electron or a muon or a kaon.
  - For the $\tau^+ \to \pi^+\pi^-\pi^+\overline{\nu}_\tau$ selection each of the tracks must be identified as a pion and not identified as an electron or a muon or a kaon.
- Signal-side π^0 multiplicity:

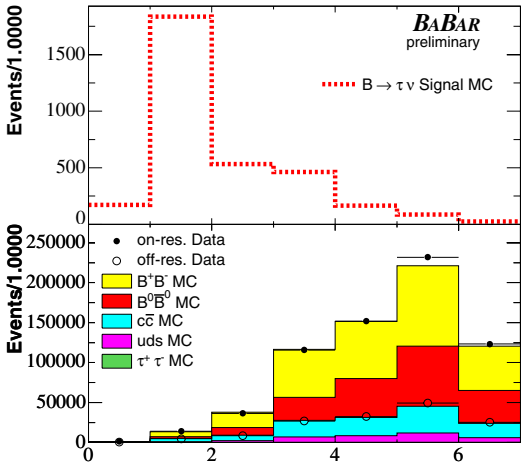

(a) Number of signal-side tracks for $D^{*0}(D^0\gamma)e\nu$ tag B candidate plotted for $B^+ \to \tau^+\nu_\tau$ signal MC simulation (top) and for data and background MC simulation (bottom).

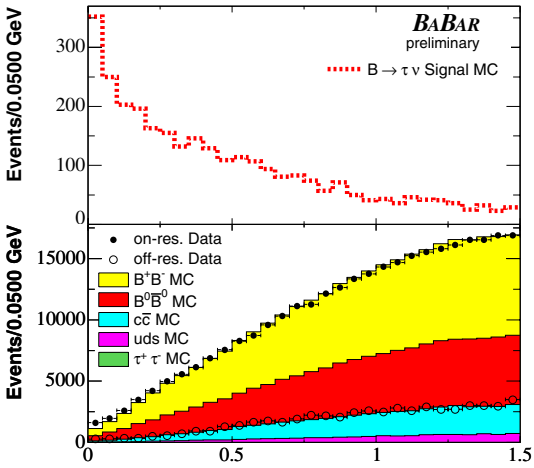

(b) $E_{\rm extra}$ distribution after the $D^{*0}(D^0\gamma)e\nu$ tag B candidate selection plotted for $B^+ \to \tau^+\nu_\tau$ signal MC simulation (top) and for data and background MC simulation (bottom).

Figure 3: The number of signal-side tracks and $E_{\rm extra}$ distributions after tag B selection, plotted for $B^+ \to \tau^+\nu_\tau$ MC simulation, background MC simulation, and data. The net charge requirement is not applied on the events plotted here. Here the simulated background events are normalized to on-resonance data luminosity. The normalization of the signal MC events is arbitrary. These distributions are similar for other tag B candidates.

  - For the $\tau^+ \to \pi^+\overline{\nu}_\tau$ selection we require the event to contain no signal-side π^0.
  - For the $\tau^+ \to \pi^+\pi^0\overline{\nu}_\tau$ selection we require that the event contains at least one signal-side π^0.

- $E_{\rm extra}$ requirement:

  - For all the signal modes $E_{\rm extra}$ must be less than 0.3 GeV.

Background consists primarily of B^+B^- events in which the tag B meson has been correctly reconstructed. The recoil side contains one or three track(s) and the additional particles which are not reconstructed by the tracking detectors or calorimeters. Typically these events contain one or more K^0_L and/or neutrinos, and frequently also additional charged or neutral particles which pass outside of the tracking and calorimeter acceptance. Background events also contain $B^0\overline{B^0}$ events. The continuum background contributes to hadronic τ decay modes. In addition some excess events in data, most likely from two-photon processes which are not modeled in MC simulation, are also seen. These backgrounds can be suppressed by the following constraints on the kinematics of the $B^+ \to \tau^+\nu_\tau$ decays.

- Missing mass: The missing mass is calculated as follows.

$$M_{\rm miss} = \sqrt{(E_{\Upsilon(4S)} - E_{\rm vis})^2 - (\vec{p}_{\Upsilon(4S)} - \vec{p}_{\rm vis})^2}. \quad (5)$$

  Here $(E_{\Upsilon(4S)}, \vec{p}_{\Upsilon(4S)})$ is the four-momenta of the $\Upsilon(4S)$, known from the beam energies. The quantities $E_{\rm vis}$ and $\vec{p}_{\rm vis}$ are the total visible energy and momentum of the event which are calculated by adding the energy and momentum, respectively, of all the reconstructed charged tracks and photons in the event.

  - For the $\tau^+ \to e^+\nu_e\overline{\nu}_\tau$ and $\tau^+ \to \mu^+\nu_\mu\overline{\nu}_\tau$ selections, events with missing mass less than 4 GeV/c^2 are rejected.
  - For the $\tau^+ \to \pi^+\overline{\nu}_\tau$ and $\tau^+ \to \pi^+\pi^0\overline{\nu}_\tau$ selections, the missing mass is required to be greater than 3 GeV/c^2.
  - For the $\tau^+ \to \pi^+\pi^-\pi^+\overline{\nu}_\tau$ selection, the missing mass is required to be greater than 2 GeV/c^2.

- Maximum CM momentum of the τ daughter:

  The following maximum CM momentum requirements are applied to the τ daughter particles.

  - The electron candidate from the $\tau^+ \to e^+\nu_e\overline{\nu}_\tau$ decay must have a CM momentum of less than 1.4 GeV/c. The CM momentum requirement is not applied to the $\tau^+ \to \mu^+\nu_\mu\overline{\nu}_\tau$ selection because of the following reason: The momentum spectrum of the lepton from τ decays peaks below 1 GeV/c. The particle identification efficiency for low momentum muons is lower than that for low momentum electrons. Therefore, applying the maximum momentum cut reduces the selection efficiency of the $\tau^+ \to \mu^+\nu_\mu\overline{\nu}_\tau$ mode significantly.
  - For the three hadronic τ decay modes, the π from $\tau^+ \to \pi^+\overline{\nu}_\tau$, the $\pi\pi^0$ combination from $\tau^+ \to \pi^+\pi^0\overline{\nu}_\tau$, or the 3π combination from $\tau^+ \to \pi^+\pi^-\pi^+\overline{\nu}_\tau$ must all have CM momenta less than 2.7 GeV/c.

The $\tau^+ \to \pi^+\pi^0\overline{\nu}_\tau$ and $\tau^+ \to \pi^+\pi^-\pi^+\overline{\nu}_\tau$ decays proceed via intermediate resonances. For these modes further background rejection can be achieved by applying the following requirements on the intermediate mesons.

- ρ^+ selection:

  The $\tau^+ \to \pi^+\pi^0\overline{\nu}_\tau$ decay proceeds via an intermediate ρ^+ state. The signal-side track is combined with a signal-side π^0 to form the ρ^+ candidate. In events with more than one signal-side π^0, the candidate with invariant mass closest to the nominal π^0 mass [4] is chosen. The invariant mass of the reconstructed ρ^+ is required to be within 0.55–1.00 GeV/c^2. A quantity similar to $\cos\theta_{B-D^{*0}\ell}$, which is defined in section 3.1, can be reconstructed for $\tau \to \rho\nu$ as follows:

$$\cos\theta_{\tau-\rho} = \frac{2E_\tau E_\rho - m_\tau^2 - m_\rho^2}{2|\vec{p}_\tau||\vec{p}_\rho|}, \quad (6)$$

  where $(E_\tau, \vec{p}_\tau)$ and $(E_\rho, \vec{p}_\rho)$ are the four-momenta in the CM frame, m_τ and m_ρ are the masses of the τ and ρ candidate, respectively. The quantities $|\vec{p}_\tau|$ and E_τ are calculated assuming that the τ is from the $B^+ \to \tau^+\nu_\tau$ decay, and that the B^+ is almost at rest in the CM frame. Candidates outside of $-1.1 < \cos\theta_{\tau-\rho} < 1.1$ are excluded.

- ρ^0 and a_1^+ selection:

  The τ decays to three charged tracks via two intermediate resonances: $\tau^+ \to a_1^+ \overline{\nu}_\tau$, $a_1^+ \to \rho^0 \pi^+$, and $\rho^0 \to \pi^+ \pi^-$. The $\pi^- \pi^+$ combination with an invariant mass closest to the nominal ρ^0 mass [4] is selected as the best ρ^0 candidate. The invariant mass of the selected ρ^0 must be within 0.55–1.00 GeV/c^2. The CM momentum of the selected ρ^0 candidate is required to be greater than 0.5 GeV/c. The invariant mass of the three signal tracks must be within 1.0–1.6 GeV/c^2. The total CM momentum of the three tracks has to be greater than 1.0 GeV/c. The three tracks are also required to converge to a common vertex and the candidates are rejected if the vertex fit probability is less than 0.1%. For $\tau \to a_1 \nu$ decay the quantity,

$$\cos\theta_{\tau-a_1} = \frac{2E_\tau E_{a_1} - m_\tau^2 - m_{a_1}^2}{2|\vec{p}_\tau||\vec{p}_{a_1}|}, \tag{7}$$

  is obtained using the similar procedure used for calculating $\cos\theta_{\tau-\rho}$. Here (E_τ, $\vec{p}_\tau$) and (E_{a_1}, $\vec{p}_{a_1}$) are the four-momenta in the CM frame, m_τ and m_{a_1} are the masses of the τ and a_1 candidate, respectively. Candidates not satisfying $-1.1 < \cos\theta_{\tau-a_1} < 1.1$ are excluded.

The signal selection criteria for all five signal modes are summarized in Table 2.

Table 2: The selection criteria for different signal modes are listed in this table. The symbols P_x^* and M_x, used in the table, correspond to the CM momentum and invariant mass of x, respectively.

$\tau^+ \to e^+\nu_e\overline{\nu}_\tau$	$\tau^+ \to \mu^+\nu_\mu\overline{\nu}_\tau$	$\tau^+ \to \pi^+\overline{\nu}_\tau$	$\tau^+ \to \pi^+\pi^0\overline{\nu}_\tau$	$\tau^+ \to \pi^+\pi^-\pi^+\overline{\nu}_\tau$
One signal-side track				Three signal-side tracks
track quality requirements for each signal track				
electron not muon not kaon	muon not electron not kaon	not electron not muon not kaon		pion not electron not muon not kaon
none	none	No signal-side π^0	Non-zero signal-side π^0	none
$E_{\rm extra} < 0.3$ GeV				
Missing Mass > 4 GeV		Missing Mass > 3 GeV		Missing Mass > 2 GeV
P^* of signal-side e track < 1.4 GeV	none	P^* of signal-side π track < 2.7 GeV	P^* of signal-side $\pi\pi^0 < 2.7$ GeV	P^* of of signal-side $3\ \pi < 2.7$ GeV
none	none	none	ρ^+ selection: $0.55 < M_{\rho^+} < 1$ GeV $-1.1 < \cos\theta_{\tau-\rho} < 1.1$	a_1^+ selection: $0.55 < M_{\pi^+\pi^-} < 1.0$ GeV $P^*_{\pi^+\pi^-} > 0.5$ GeV $1.0 < M_{3\pi} < 1.6$ GeV $P^*_{3\pi} > 1.0$ GeV Vertex prob. of 3 tracks $> 1\%$ $-1.1 < \cos\theta_{\tau-a_1} < 1.1$

3.2.1 SIGNAL EFFICIENCY

The "signal-side selection efficiencies" for the τ decay modes are determined from signal MC simulation and summarized in Table 3. For each τ selection mode, the signal-side efficiency (ε_i, where $i \equiv$ selection mode) is computed as the ratio of the number of events surviving the requirements

of that selection mode to the number of events where a tag B meson is reconstructed. In the computation of the total signal-side efficiency for each selection we take into account the cross-feed from other τ decay modes reported in Table 3.

The selection efficiency for $\tau^+ \to \mu^+\nu_\mu\overline{\nu}_\tau$ is low compared to that of the $\tau^+ \to e^+\nu_e\overline{\nu}_\tau$ mode, because of the fact that the momentum spectrum of the signal muons peaks below 1 GeV/c, where the muon detection efficiency is low. Since no minimum momentum requirement and no tight pion identification criteria are applied to the $\tau^+ \to \pi^+\overline{\nu}_\tau$ signal selection, electron and muon signal tracks that fail particle identification requirement get selected in this mode. Any true $\tau^+ \to \pi^+\pi^0\overline{\nu}_\tau$ signal events, with a missed π^0 also get included in $\tau^+ \to \pi^+\overline{\nu}_\tau$ selection mode. Therefore the $\tau^+ \to \pi^+\overline{\nu}_\tau$ selection mode has the highest signal efficiency. From MC estimation we expect $\sim$10 signal events at 112.5 fb^{-1}, assuming $\mathcal{B}(B^+ \to \tau^+\nu_\tau) = 10^{-4}$.

Table 3: Efficiency of the different selections (columns) for the most abundant τ decay modes (rows). The last two rows show the total efficiency for each selection weighted by the decay branching fractions, and the total efficiency. The errors are statistical only. The total efficiency for each selection is $\varepsilon_i = \Sigma_{j=1}^{8}\varepsilon_i^j f_j$, where ε_i^j is the efficiency of the selection i for the simulated τ decay mode j. The index j corresponds to the different τ decay mode in the MC simulation, and $f_j = \mathcal{B}(\tau \to j)$ are the τ branching fractions from Ref. [4]. If the efficiency is zero a 90% upper limit is quoted.

τ decay mode in Monte Carlo simulation	$e\nu\nu$ selection efficiency (%)	$\mu\nu\nu$ selection efficiency (%)	$\pi\nu$ selection efficiency (%)	$\pi\pi^0\nu$ selection efficiency (%)	$\pi\pi\pi\nu$ selection efficiency (%)
$e\nu\overline{\nu}$	48.6 $\pm$ 2.8	0.1 $\pm$ 0.1	11.9 $\pm$ 1.2	0.1 $\pm$ 0.1	0 ($<$ 0.2)
$\mu\nu\overline{\nu}$	0.1 $\pm$ 0.1	25.8 $\pm$ 1.9	53.3 $\pm$ 3.0	0.7 $\pm$ 0.3	0 ($<$ 0.3)
$\pi\nu$	0 ($<$ 0.4)	0.5 $\pm$ 0.3	57.5 $\pm$ 4.0	2.6 $\pm$ 0.7	0 ($<$ 0.4)
$\pi\pi^0\nu$	0 ($<$ 0.2)	0.3 $\pm$ 0.1	12.1 $\pm$ 1.0	8.8 $\pm$ 0.8	0 ($<$ 0.2)
$\pi\pi\pi\nu$	0 ($<$ 0.5)	0 ($<$ 0.5)	1.1 $\pm$ 0.6	0 ($<$ 0.5)	27.6 $\pm$ 3.2
$\pi\pi^0\pi^0\nu$	0 ($<$ 0.5)	0 ($<$ 0.5)	2.8 $\pm$ 0.8	2.8 $\pm$ 0.8	0 ($<$ 0.5)
$\pi\pi\pi\pi^0\nu$	0 ($<$ 1.0)	0 ($<$ 1.0)	0.5 $\pm$ 0.5	0 ($<$ 1.0)	4.1 $\pm$ 1.5
other	1.2 $\pm$ 0.5	2.1 $\pm$ 0.7	10.0 $\pm$ 1.5	2.5 $\pm$ 0.7	1.0 $\pm$ 0.4
all τ decay	8.4 $\pm$ 0.4	4.8 $\pm$ 0.3	21.9 $\pm$ 0.7	3.2 $\pm$ 0.2	2.1 $\pm$ 0.2
Total	40.4 $\pm$ 0.9				

3.2.2 EXPECTED BACKGROUND FROM MONTE CARLO SIMULATION

To obtain the background estimation from the MC simulation, $B\overline{B}$ and $e^+e^- \to u\overline{u}$, $d\overline{d}$, $s\overline{s}$, $c\overline{c}$, and $\tau^+\tau^-$ events are scaled to equivalent luminosity in data. The estimated background in different selection modes is listed in Table 4. The three modes $\tau^+ \to e^+\nu_e\overline{\nu}_\tau$, $\tau^+ \to \mu^+\nu_\mu\overline{\nu}_\tau$, $\tau^+ \to \pi^+\overline{\nu}_\tau$ are relatively clean compared to the other two selection modes. Signal to background ratios in $\tau^+ \to e^+\nu_e\overline{\nu}_\tau$, $\tau^+ \to \mu^+\nu_\mu\overline{\nu}_\tau$, and $\tau^+ \to \pi^+\overline{\nu}_\tau$ selection modes are 10:59, 10:75, and 10:85 respectively, assuming $\mathcal{B}(B^+ \to \tau^+\nu_\tau) = 10^{-4}$. For the $\tau^+ \to \pi^+\pi^0\overline{\nu}_\tau$ and $\tau^+ \to \pi^+\pi^-\pi^+\overline{\nu}_\tau$ modes the signal to background ratio is 10:354 and 10:513, respectively.

Table 4: Expected final raw background and signal yield at $112.5\,\mathrm{fb}^{-1}$ estimated from background and signal MC simulation. No systematic correction is applied on simulated events. The listed errors are statistical only. If the efficiency is zero a 90% upper limit on the expected background is quoted.

	$e^+\nu_e\overline{\nu}_\tau$	$\mu^+\nu_\mu\overline{\nu}_\tau$	$\pi^+\overline{\nu}_\tau$	$\pi^+\pi^0\overline{\nu}_\tau$	$\pi^+\pi^-\pi^+\overline{\nu}_\tau$
B^+B^-	8.29 ± 1.69	7.25 ± 1.58	24.18 ± 2.89	14.16 ± 2.21	14.16 ± 2.21
$B^0\overline{B}^0$	3.36 ± 0.97	1.40 ± 0.63	8.11 ± 1.51	3.64 ± 1.01	7.83 ± 1.48
Combined $B\overline{B}$	11.65 ± 1.95	8.65 ± 1.70	32.29 ± 3.26	17.80 ± 2.43	21.99 ± 2.66
$c\overline{c}$	0 (< 2.2)	0 (< 2.2)	9.54 ± 3.02	8.59 ± 2.86	2.86 ± 1.65
$u\overline{u}$, $d\overline{d}$, $s\overline{s}$	0 (< 1.9)	0 (< 1.9)	0 (< 1.9)	0 (< 1.9)	0.81 ± 0.81
$\tau^+\tau^-$	0.48 ± 0.48	0 (< 1.1)	2.87 ± 1.17	0.48 ± 0.48	0 (< 1.1)
Combined non $B\overline{B}$	0.48 ± 0.48	0	12.41 ± 3.24	9.07 ± 2.90	3.67 ± 1.84
Total Background	12.12 ± 2.01	8.65 ± 1.70	44.69 ± 4.59	26.86 ± 3.79	25.67 ± 3.24
Expected signal events for $\mathcal{B}(B^+ \to \tau^+\nu_\tau) = 10^{-4}$	2.03 ± 0.10	1.16 ± 0.07	5.26 ± 0.16	0.76 ± 0.06	0.50 ± 0.05

3.2.3 BACKGROUND ESTIMATION FROM E_{extra} SIDE BAND IN DATA

The $E_{\mathrm{extra}} < 0.3$ GeV region is defined as the "signal region" and the $0.35 < E_{\mathrm{extra}} < 1.0$ GeV region is defined as the "side band". The E_{extra} shape in the MC distribution is used to extrapolate the data side band to the signal region.

The number of MC events in signal region ($N^{\mathrm{MC}}_{\mathrm{Sig}}$) and side band ($N^{\mathrm{MC}}_{\mathrm{SideB}}$) are counted and their ratio (R_{MC}) is obtained.

$$R_{\mathrm{MC}} \;=\; \frac{N^{\mathrm{MC}}_{\mathrm{Sig}}}{N^{\mathrm{MC}}_{\mathrm{SideB}}}$$

Using the number of data events in the side band ($N^{\mathrm{data}}_{\mathrm{SideB}}$) and the ratio R_{MC}, the number of expected background events in the signal region in data ($N^{\mathrm{data}}_{\mathrm{SideB}}$) is estimated.

$$N^{\mathrm{data}}_{\mathrm{SideB}} \;=\; N^{\mathrm{data}}_{\mathrm{SideB}} \cdot R_{\mathrm{MC}}$$

The background estimation for the different selection modes from the E_{extra} side band extrapolation are shown in Table 5. The number of estimated background events in the signal region from the data side band extrapolation are in agreement with the background estimation from MC simulation within statistical uncertainty.

Table 5: Background estimation in the signal region ($E_{\rm extra} < 0.3$ GeV) for the different selection modes.

Selection	$N^{\rm MC}_{\rm SideB}$	$N^{\rm MC}_{\rm Sig}$	$R_{\rm MC}$	$N^{\rm data}_{\rm SideB}$	$N^{\rm exp}_{\rm Sig}$
$e^+\nu_e\overline{\nu}_\tau$	83.63 ± 5.67	12.12 ± 2.01	0.14 ± 0.03	103.00 ± 10.15	14.93 ± 3.05
$\mu^+\nu_\mu\overline{\nu}_\tau$	64.18 ± 4.83	8.65 ± 1.70	0.13 ± 0.03	53.00 ± 7.28	7.14 ± 1.80
$\pi^+\overline{\nu}_\tau$	227.09 ± 10.86	44.69 ± 4.59	0.20 ± 0.02	250.00 ± 15.81	49.20 ± 6.39
$\pi^+\pi^0\overline{\nu}_\tau$	179.44 ± 9.37	26.86 ± 3.79	0.15 ± 0.02	182.00 ± 13.49	27.24 ± 4.57
$\pi^+\pi^-\pi^+\overline{\nu}_\tau$	218.59 ± 9.55	25.67 ± 3.24	0.12 ± 0.02	199.00 ± 14.11	23.37 ± 3.53

4 VALIDATION OF $E_{\rm extra}$ SIMULATION

The $E_{\rm extra}$ distribution in signal and background MC simulation are validated using various control samples. We compare the $E_{\rm extra}$ distributions between on-resonance data and MC simulation, in both signal region and side band, using the control samples. Agreement between the distributions would provide validation of the $E_{\rm extra}$ modeling in the simulation.

4.1 $E_{\rm extra}$ IN THE SIGNAL MONTE CARLO SIMULATION

The "double-tagged" events, for which both of the B mesons are reconstructed in tagging modes, $B^- \to D^{*0}\ell^-\overline{\nu}_\ell$ vs $B^+ \to \overline{D}^{*0}\ell^+\nu_\ell$, are used as a control sample to validate the $E_{\rm extra}$ simulation. Due to the large branching fraction and high tagging efficiency for these events, a sizable sample of such events is reconstructed in the on-resonance dataset. These double-tag events contain very little background due to the full reconstruction of the event.

To select double-tag events we require that the two tag B candidates do not share any tracks or neutrals. If there are more than two such non-overlapping tag B candidates in the event then the best two are selected using the same best candidate selection criteria, as described in Sec. 3.1. After selecting the two tag B candidates only the events with no extra charged tracks are selected.

The $E_{\rm extra}$ for the double-tagged sample is calculated by summing the CM energy of the photons which are not associated with either of the tag B candidates. The sources of neutrals contributing to the $E_{\rm extra}$ distribution in double-tagged events are similar to those contributing to the $E_{\rm extra}$ distribution in the signal MC simulation. Therefore the agreement of the $E_{\rm extra}$ distribution between data and MC simulation for the double-tagged sample, in figure 4, is used as a validation of the $E_{\rm extra}$ simulation in the signal MC.

4.2 $E_{\rm extra}$ IN THE BACKGROUND MONTE CARLO SIMULATION

The following two background control samples are used to study the agreement between data and simulation in the $E_{\rm extra} < 0.35$ GeV region.

- Events with two remaining signal-side tracks
- Events with non-zero net charge

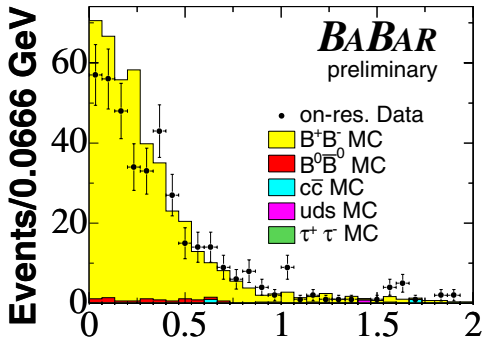

Figure 4: The distribution of the remaining neutral energy ($E_{\rm extra}$) for double-tagged events, plotted for simulation and data.

The procedure from Sec. 3.2.3, the background estimation from the $E_{\rm extra}$ side band, is used for this test. In Table 6 we show the comparison of the number of expected data events ($N^{\rm data}_{\rm SideB}$) in the signal region with the observed number of data events ($N^{\rm obs}_{\rm Sig}$) in the signal region. The agreement between the above two quantities provides validation of background estimation in the low $E_{\rm extra}$ region.

Table 6: Test of background estimation in the low $E_{\rm extra}$ region from various control samples. Signal selection cuts for different τ decay modes are applied on the control samples. The expected and observed number of events in the signal region agree within error for all the samples ($P(\chi^2) = 0.15$ between the entries in the last two columns. Here $\chi^2 = 10.77$, and the number of degrees of freedom is 7.).

Selection	$N^{\rm MC}_{\rm SideB}$	$N^{\rm data}_{\rm SideB}$	$N^{\rm MC}_{\rm Sig}$	$N^{\rm exp}_{\rm Sig}$	$N^{\rm obs}_{\rm Sig}$
Two signal-side track control sample					
$e\nu\overline{\nu}$	223.34 ± 8.68	203.00 ± 14.25	76.91 ± 5.12	69.90 ± 7.29	64.00 ± 8.00
$\mu\nu\overline{\nu}$	144.80 ± 7.14	123.00 ± 11.09	57.68 ± 4.43	49.00 ± 6.29	55.00 ± 7.42
$\pi\nu$	1132.39 ± 21.64	1050.00 ± 32.40	401.89 ± 12.53	372.65 ± 17.83	422.00 ± 20.54
$\pi\pi^0\nu$	1175.99 ± 21.78	959.00 ± 30.97	241.36 ± 9.70	196.83 ± 10.78	232.00 ± 15.23
$Q_{net} \neq 0$ control sample					
$e\nu\overline{\nu}$	16.86 ± 2.33	8.00 ± 2.83	4.10 ± 1.14	1.94 ± 0.92	5.00 ± 2.24
$\mu\nu\overline{\nu}$	6.66 ± 1.46	2.00 ± 1.41	2.29 ± 0.87	0.69 ± 0.57	0
$\pi\nu$	68.62 ± 5.31	63.00 ± 7.94	23.26 ± 2.83	21.36 ± 4.09	24.00 ± 4.90
$\pi\pi^0\nu$	63.14 ± 5.14	44.00 ± 6.63	9.14 ± 1.74	6.37 ± 1.63	6.00 ± 2.45

5 STUDIES OF SYSTEMATICS

The main sources of uncertainty in the determination of the $B^+ \to \tau^+\nu_\tau$ branching fraction are the following:

- We divide the uncertainties in signal efficiency determination into two categories.
  - Uncertainty in tagging efficiency determination
  - Uncertainty in determination of the efficiency ε_i for each selection mode.
- Uncertainty in the determination of the number of expected background events in the signal region for each selection mode.

A small uncertainty of 1.1% also enters the branching ratio limit calculation from the estimation of the number of B^+B^- events present in the data sample [13].

5.1 TAGGING EFFICIENCY SYSTEMATICS

The tagging efficiency and yield in signal simulation is corrected using the "double-tagged" events. The selection of "double-tagged" events is described in sec. 4.1.

The number of double-tagged events (N_2) is given by

$$N_2 \;=\; \varepsilon^2 N \tag{8}$$

where ε is the efficiency and N is the original number of events. The double tag yield in data is 407.0 $\pm$ 20.2. In the simulation, we find 434.4 $\pm$ 12.4 double-tags, with very few non-B^+B^- events. The expected number of B^+B^- events in the dataset is $N = (62.06 \pm 0.68) \times 10^6$ events. Calculating the efficiency using the numbers of double-tags in data and normalized MC in equation 8, we find the efficiencies $\varepsilon_{\rm data}$ and $\varepsilon_{\rm MC}$. The correction factor, ratio of the efficiencies between data and simulation, from this method is

$$\frac{\varepsilon_{\rm data}}{\varepsilon_{\rm MC}} \;=\; 0.969 \pm 0.029.$$

The correction factor obtained from the double tags agrees within error with the normalization factor used in section 3.1 to correct tag B meson yield in simulation. Therefore, the double tags provide the validation for the tag B yield correction. We take the 3.1% error obtained from the double tag method as the systematic error associated with the tagging efficiency and yield correction in Monte Carlo.

5.2 UNCERTAINTIES IN THE SIGNAL SELECTION EFFICIENCIES IN EACH SELECTION MODE

Besides tagging efficiency uncertainty, the contribution to the systematic uncertainties in the determination of the efficiencies comes from systematic uncertainty on the tracking efficiency, particle identification, and simulation of the neutral clusters in the calorimeter which contribute to the $E_{\rm extra}$ distribution. Uncertainty in the π^0 reconstruction efficiency introduces an additional contribution to the systematics in the $\tau^+ \to \pi^+\overline{\nu}_\tau$ (5.0%) and $\tau^+ \to \pi^+\pi^0\overline{\nu}_\tau$ (7.7 %) selection modes. The different contributions to the systematic uncertainty on the selection efficiencies are listed in table 7.

Table 7: Contribution to the systematic uncertainty on the signal selection efficiencies in different selection modes.

Selection modes	tracking (%)	Particle Identification (%)	Neutral Reconstruction (%)	Total Systematic Error (%)	Correction Factor
$e^+\nu_e\overline{\nu}_\tau$	1.4	0.1	3.1	3.4	0.99
$\mu^+\nu_\mu\overline{\nu}_\tau$	1.4	3.0	2.3	4.0	0.89
$\pi^+\overline{\nu}_\tau$	1.4	0.5	$3.1 \oplus 5.0$	6.1	1.02
$\pi^+\pi^0\overline{\nu}_\tau$	1.4	0.1	$2.9 \oplus 7.7$	8.3	0.95
$\pi^+\pi^-\pi^+\overline{\nu}_\tau$	4.2	0.3	4.7	6.3	1.00

5.3 UNCERTAINTIES IN THE BACKGROUND ESTIMATION

The background estimation is performed by extrapolating the number of events in the $E_{\rm extra}$ side band in data into the signal region as described in sec. 3.2.3. The major uncertainty related to background estimation comes from the data and MC statistics. The modeling of the $E_{\rm extra}$ variable in the background MC contributes to additional systematic corrections to the background estimation. The systematic corrections due to $E_{\rm extra}$ modeling for different modes are the following: (1.02 ± 0.04) for $\tau^+ \to e^+\nu_e\overline{\nu}_\tau$, (1.13 ± 0.06) for $\tau^+ \to \mu^+\nu_\mu\overline{\nu}_\tau$, (1.12 ± 0.03) for $\tau^+ \to \pi^+\overline{\nu}_\tau$, (1.09 ± 0.04) for $\tau^+ \to \pi^+\pi^0\overline{\nu}_\tau$ and (1.07 ± 0.03) for $\tau^+ \to \pi^+\pi^-\pi^+\overline{\nu}_\tau$.

6 RESULTS

After finalizing the signal selection criteria, the signal region ($E_{\rm extra} < 0.3\,{\rm GeV}$) in the on-resonance data is examined. Table 8 lists the number of observed events in on-resonance data in the signal region, together with the expected number of background events in the signal region. Figure 5 shows the $E_{\rm extra}$ distribution in data and simulation. In almost all the modes the observed number of events is in agreement with the expected number of background events.

Table 8: Shown are the observed number of on-resonance data events in the signal region, together with number of expected background events. The background estimations include systematic corrections referred to in Sec. 5.3.

Selection	Expected Background Events	Observed Events in On-resonance Data
$e^+\nu_e\overline{\nu}_\tau$	15.15 ± 3.14	13
$\mu^+\nu_\mu\overline{\nu}_\tau$	8.05 ± 2.07	10
$\pi^+\overline{\nu}_\tau$	55.30 ± 7.37	72
$\pi^+\pi^0\overline{\nu}_\tau$	29.80 ± 5.10	30
$\pi^+\pi^-\pi^+\overline{\nu}_\tau$	25.10 ± 3.87	26

We determine the $B^+ \to \tau^+\nu_\tau$ branching fraction from the number of signal candidates s_i in data for each τ decay mode, according to $s_i = N_{B\overline{B}}\mathcal{B}(B^+ \to \tau^+\nu_\tau)\varepsilon_{\rm tag}\varepsilon_i$. Here $N_{B\overline{B}}$ is the total number of $B\overline{B}$ pairs in data, $\varepsilon_{\rm tag}$ is the tag reconstruction efficiency in signal MC; ε_i is

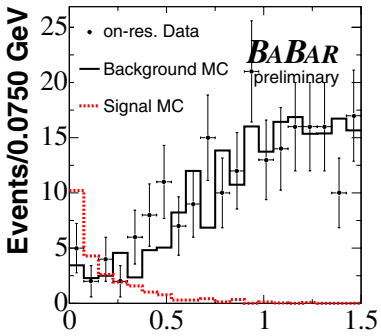

(a) The distribution of the $E_{\rm extra}$ for events satisfying $\tau^+ \to e^+\nu_e\overline{\nu}_\tau$ selection.

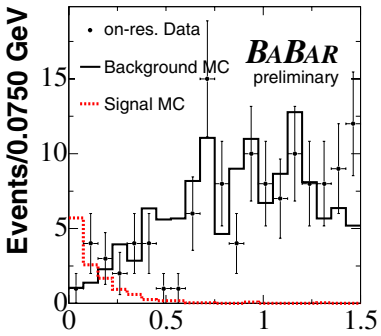

(b) The distribution of the $E_{\rm extra}$ for events satisfying $\tau^+ \to \mu^+\nu_\mu\overline{\nu}_\tau$ selection.

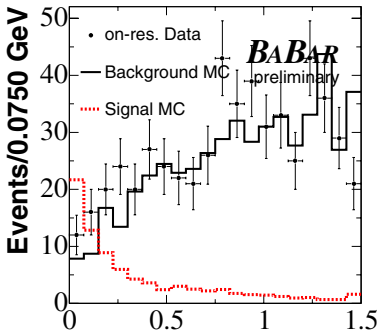

(c) The distribution of the $E_{\rm extra}$ for events satisfying $\tau^+ \to \pi^+\overline{\nu}_\tau$ selection.

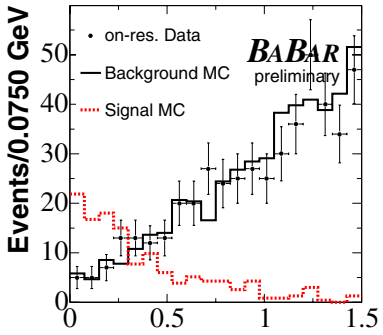

(d) The distribution of the $E_{\rm extra}$ for events satisfying $\tau^+ \to \pi^+\pi^0\overline{\nu}_\tau$ selection.

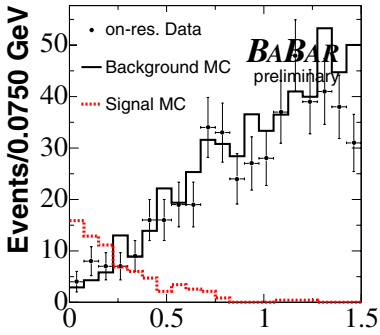

(e) The distribution of the $E_{\rm extra}$ for events satisfying $\tau^+ \to \pi^+\pi^-\pi^+\overline{\nu}_\tau$ selection.

Figure 5: The distribution of the $E_{\rm extra}$ for events passing the selections for different τ decay modes, plotted for background and signal MC simulation and on-resonance data. Events plotted here are required to pass selections for corresponding signal modes. The background MC events are normalized to on-resonance data luminosity. The signal MC events for the $\tau^+ \to e^+\nu_e\overline{\nu}_\tau$, $\tau^+ \to \mu^+\nu_\mu\overline{\nu}_\tau$, and $\tau^+ \to \pi^+\overline{\nu}_\tau$ modes are normalized assuming $\mathcal{B}(B^+ \to \tau^+\nu_\tau) = 10^{-3}$, whereas for the normalization of the signal MC events in the $\tau^+ \to \pi^+\pi^0\overline{\nu}_\tau$ and $\tau^+ \to \pi^+\pi^-\pi^+\overline{\nu}_\tau$ modes we use $\mathcal{B}(B^+ \to \tau^+\nu_\tau) = 10^{-2}$. The above $\mathcal{B}(B^+ \to \tau^+\nu_\tau)$ assumptions for the normalization of the signal MC events are used to compare the shapes of the $E_{\rm extra}$ distributions between signal MC events, background MC simulation, and on-resonance data events.

the signal-side selection efficiency in different τ decay modes calculated with respect to the total number of reconstructed tag B mesons. Table 9 shows the values of $N_{B\overline{B}}$, $\varepsilon_{\rm tag}$ and ε_i, after applying appropriate systematic corrections (sec. 5).

Table 9: Shown are the values for the quantities $N_{B\overline{B}}$, $\varepsilon_{\rm tag}$ and ε_i, after applying systematic corrections.

	Value	Total Uncertainty (%)
$N_{B\overline{B}}$	$(124.1 \pm 1.4) \times 10^6$	1.1
$\varepsilon_{\rm tag}$	$(1.82 \pm 0.074 \pm 0.055) \times 10^{-3}$	5.06
$\varepsilon_{e^+\nu_e\overline{\nu}_\tau}$	$(8.36 \pm 0.42 \pm 0.28)$ %	6.03
$\varepsilon_{\mu^+\nu_\mu\overline{\nu}_\tau}$	$(4.30 \pm 0.28 \pm 0.17)$ %	7.56
$\varepsilon_{\pi^+\overline{\nu}_\tau}$	$(22.34 \pm 0.72 \pm 1.36)$ %	6.91
$\varepsilon_{\pi^+\pi^0\overline{\nu}_\tau}$	$(3.01 \pm 0.24 \pm 0.25)$ %	11.45
$\varepsilon_{\pi^+\pi^-\pi^+\overline{\nu}_\tau}$	$(2.07 \pm 0.20 \pm 0.13)$ %	11.53

The results from each decay mode are combined using the ratio $Q = \mathcal{L}(s+b)/\mathcal{L}(b)$, where $\mathcal{L}(s+b)$ and $\mathcal{L}(b)$ are the likelihood functions for signal plus background and background-only hypotheses, respectively [14, 15]:

$$\mathcal{L}(s+b) \equiv \prod_{i=1}^{n_{ch}} \frac{e^{-(s_i+b_i)}(s_i+b_i)^{n_i}}{n_i!},\ \mathcal{L}(b) \equiv \prod_{i=1}^{n_{ch}} \frac{e^{-b_i} b_i^{n_i}}{n_i!}, \tag{9}$$

Since we have no evidence of signal we set an upper limit. The statistical and systematic uncertainties on the expected background (b_i) are included in the likelihood definition by convolving it with a Gaussian distribution ($\mathcal{G}$). The mean of $\mathcal{G}$ is b_i, and the standard deviation (σ_{b_i}) of $\mathcal{G}$ is the statistical and systematic errors on b_i added in quadrature [16],

$$\mathcal{L}(s_i+b_i) \rightarrow \mathcal{L}(s_i+b_i) \otimes \mathcal{G}(b_i, \sigma_{b_i}) \tag{10}$$

(similarly for $\mathcal{L}(b_i)$). We determine the limit on the branching fraction to be $\mathcal{B}(B^+ \rightarrow \tau^+\nu_\tau) < 4.3 \times 10^{-4}$ at the 90% C.L. Figure 6 shows the likelihood ratios as a function of $\mathcal{B}(B^+ \rightarrow \tau^+\nu_\tau)$. The solid curve corresponds to the case in which the uncertainty on the expected background is not included. The effect of including the uncertainty on the expected background can be seen from the dashed curve.

The measured branching fraction, the value that maximizes the likelihood ratio estimator is $1.9^{+1.8}_{-1.7} \times 10^{-4}$.

The *BABAR* Collaboration performed also a search for the $B^+ \rightarrow \tau^+\nu_\tau$ decay [9], where the tag B mesons are reconstructed in hadronic modes $B^- \rightarrow D^{(*)0}X^-$. Here X^- represents a combination of up to five charged pions or kaons and up to two π^0 candidates. The hadronic reconstruction analysis is statistically independent from the current analysis and has obtained a limit $\mathcal{B}(B^+ \rightarrow \tau^+\nu_\tau) < 4.2 \times 10^{-4}$ at the 90% C.L. We combine the results from the statistically independent hadronic and semi-leptonic samples by first calculating the likelihood ratio estimator, $Q \equiv \mathcal{L}(s+b)/\mathcal{L}(b)$ using the likelihood functions from each method. We then create a combined estimator from the product of the semi-leptonic ($Q_{\rm sl}$) and hadronic ($Q_{\rm had}$) likelihood ratio estimators, $Q = Q_{\rm sl} \times Q_{\rm had}$. The combined upper limit on the branching fraction is $\mathcal{B}(B^+ \rightarrow \tau^+\nu_\tau) < 3.3 \times 10^{-4}$ at the 90% C.L.

Using equation 1, the combined branching fraction upper limit, and the measured value of $|V_{ub}|$ [4] we set a limit on f_B. We find $f_B < 0.480$ GeV at 90% C.L.

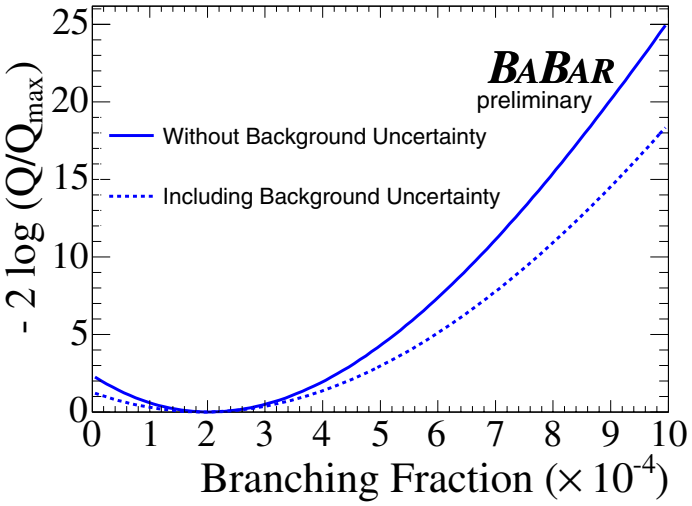

Figure 6: The distribution of likelihood ratio as a function of $\mathcal{B}(B^+ \to \tau^+\nu_\tau)$. The dashed (solid) curves corresponds to the case in which the uncertainty on the expected background is included (not included).

The *BABAR* Collaboration also searched for $B^+ \to \tau^+\nu_\tau$ decays using semi-exclusive semi-leptonic decay modes $B^- \to D^0\ell^-\bar{\nu}_\ell X$ where $\ell = e, \mu$ and X can be a γ, π^0, or nothing [9]. In the signal-side only the leptonic τ decays, $\tau^+ \to e^+\nu_e\overline{\nu}_\tau$ and $\tau^+ \to \mu^+\nu_\mu\overline{\nu}_\tau$, are identified. The $B^- \to D^{*0}\ell^-\overline{\nu}_\ell$ tags used in this current analysis overlap with the $B^- \to D^0\ell^-\bar{\nu}_\ell X$ tags and the analyses are therefore not combined.

7 SUMMARY

We have performed a search for the decay process $B^+ \to \tau^+\nu_\tau$. To accomplish this a sample of semi-leptonic B decays ($D^{*0}\ell^-\overline{\nu}_\ell$) has been used to reconstruct one of the B mesons and the remaining information in the event is searched for evidence of $B^+ \to \tau^+\nu_\tau$. We find no evidence for this decay process and set a preliminary limit on its branching fraction of

$$\mathcal{B}(B^+ \to \tau^+\nu_\tau) \quad < \quad 4.3 \times 10^{-4} \text{ at the } 90\% \text{ CL.}$$

By combining this analysis with a statistically independent $B^+ \to \tau^+\nu_\tau$ search performed using a hadronic B reconstruction we find the preliminary combined limit:

$$\mathcal{B}(B^+ \to \tau^+\nu_\tau)_{combined} < 3.3 \times 10^{-4} \text{ at the } 90\% \text{ CL.}$$

8 ACKNOWLEDGMENTS

We are grateful for the extraordinary contributions of our PEP-II colleagues in achieving the excellent luminosity and machine conditions that have made this work possible. The success of this project also relies critically on the expertise and dedication of the computing organizations that support *BABAR*. The collaborating institutions wish to thank SLAC for its support and the

kind hospitality extended to them. This work is supported by the US Department of Energy and National Science Foundation, the Natural Sciences and Engineering Research Council (Canada), Institute of High Energy Physics (China), the Commissariat à l'Energie Atomique and Institut National de Physique Nucléaire et de Physique des Particules (France), the Bundesministerium für Bildung und Forschung and Deutsche Forschungsgemeinschaft (Germany), the Istituto Nazionale di Fisica Nucleare (Italy), the Foundation for Fundamental Research on Matter (The Netherlands), the Research Council of Norway, the Ministry of Science and Technology of the Russian Federation, and the Particle Physics and Astronomy Research Council (United Kingdom). Individuals have received support from CONACyT (Mexico), the A. P. Sloan Foundation, the Research Corporation, and the Alexander von Humboldt Foundation.

References

[1] N. Cabbibo, Phys. Rev. Lett. **10**, 531 (1963).

[2] M. Kobayashi and T. Maskawa, Prog. Theor. Phys. **49**, 652 (1972).

[3] W.-S. Hou, Phys. Rev. D **48**, 2342 (1993).

[4] Particle Data Group, S. Eidelman *et al.*, Phys. Lett. B **592**, 1 (2004).

[5] CLEO Collaboration, T. E. Browder *et al.*, Phys. Rev. Lett. **86**, 2950 (2001).

[6] L3 Collaboration, M Acciarri *et al.*, Phys. Lett. B **396**, 327 (1997).

[7] ALEPH Collaboration, D. Buskulic *et al.*, Phys. Lett. B **343**, 444 (1995).

[8] DELPHI Collaboration, P Abreu *et al.*, Phys. Lett. B **496**, 43 (2000).

[9] *BABAR* Collaboration, B. Aubert *et al.*, "A Search for the Rare Leptonic Decay $B^- \to \tau^- \overline{\nu}_\tau$", submitted to Phys. Rev. Lett. (hep-ex/0407038).

[10] The *BABAR* Collaboration, B. Aubert *et al.*, Nucl. Instr. Meth. A **479**, 1 (2002).

[11] S. Agostinelli *et al.*, "Geant4 - A Simulation Toolkit", Nucl. Instr. Meth. A **506**, 250 (2003).

[12] G. C. Fox and S. Wolfram, Phys. Rev. Lett. **41**, 1581 (1978).

[13] The *BABAR* Collaboration, B. Aubert *et al.*, Phys. Rev. D **67**, 032002 (2003).

[14] A. L. Read, J. Phys. **G28**, 2693 (2002).

[15] ALEPH Collaboration and DELPHI Collaboration and L3 Collaboration and OPAL Collaboration and LEP Working Group for Higgs boson searches, R. Barate et al., Phys. Lett. B **565**, 61 (2003).

[16] L. Lista, Nucl. Instr. Meth. A **517**, 360 (2004).